metals

MDPI

Article

Welding of Ti6Al4V and Al6082-T6 Alloys by a Scanning Electron Beam

Angel Anchev [1,*], Darina Kaisheva [2,3], Georgi Kotlarski [2], Vladimir Dunchev [1], Borislav Stoyanov [4], Maria Ormanova [2], Milka Atanasova [1], Vladimir Todorov [1], Petya Daskalova [4] and Stefan Valkov [2,5]

[1] Department of Material Science and Mechanics of Materials, Technical University of Gabrovo, 4 H. Dimitar Str., 5300 Gabrovo, Bulgaria; v.dunchev@tugab.bg (V.D.); matanasova@tugab.bg (M.A.); v_p_todorov@abv.bg (V.T.)
[2] Institute of Electronics, Bulgarian Academy of Sciences, 72 Tzarigradsko Chausse Blvd, 1784 Sofia, Bulgaria; darinakaisheva@ie.bas.bg (D.K.); gvkotlarski@gmail.com (G.K.); m.ormanova@ie.bas.bg (M.O.); stsvalkov@gmail.com (S.V.)
[3] Department of Physics, South-West University, Neofit Rilski, 66 Ivan Michailov Str., 2700 Blagoevgrad, Bulgaria
[4] Department of Industrial Design and Textile Engineering, Technical University of Gabrovo, 4 H. Dimitar Str., 5300 Gabrovo, Bulgaria; stoyanov_b@mail.bg (B.S.); p.daskalova@tugab.bg (P.D.)
[5] Department of Mathematics, Informatics, and Natural Sciences, Technical University of Garbovo, 4 H. Dimitar Str., 5300 Gabrovo, Bulgaria
* Correspondence: anchev@tugab.bg

Abstract: This work presents the results of an investigation into the influence of beam offset on the structure and mechanical properties of electron-beam-welded joints between Ti6Al4V and Al6082-T6 alloys. The experimental procedure involved the use of specific technological conditions: an accelerating voltage of 60 kV, an electron beam current of 35 mA, a specimen motion speed of 10 mm/s, and a beam offset of 0.5 mm towards both alloys, as well as welding without an offset. The phase composition of the joints was analyzed using X-ray diffraction (XRD). The microstructure and chemical composition of the seams were studied by scanning electron microscopy (SEM) and energy-dispersive X-ray spectroscopy (EDX). The results obtained for the structure of the joints show that the beam offset has a significant influence on the structure. The microhardness was studied by means of the Vickers method. The results for the microstructure showed that the welding procedure without offset and with an offset towards the Ti alloy leads to inhomogeneous welded joints with a significant amount of intermetallics. The offset towards the Al alloy leads to the formation of a narrow area of $TiAl_3$ phase. The measured microhardness corresponds to the increased amount of intermetallics in the case of offset towards the Ti alloy, with which the highest values were presented (about 58% higher than with Ti6Al4V plate). The results obtained for tensile properties show that the offset to the Al6082-T6 alloy leads to the highest values of tensile strength (TS) and yield strength (YS), which are twice higher than in welding without offsetting of the electron beam.

Keywords: electron-beam welding; titanium alloy; aluminum alloy; structure; mechanical properties

check for updates

Citation: Anchev, A.; Kaisheva, D.; Kotlarski, G.; Dunchev, V.; Stoyanov, B.; Ormanova, M.; Atanasova, M.; Todorov, V.; Daskalova, P.; Valkov, S. Welding of Ti6Al4V and Al6082-T6 Alloys by a Scanning Electron Beam. *Metals* **2023**, *13*, 1252. https://doi.org/10.3390/met13071252

Academic Editors: Jiankang Huang and António Bastos Pereira

Received: 1 June 2023
Revised: 28 June 2023
Accepted: 7 July 2023
Published: 9 July 2023

Copyright: © 2023 by the authors. Licensee MDPI, Basel, Switzerland. This article is an open access article distributed under the terms and conditions of the Creative Commons Attribution (CC BY) license (https://creativecommons.org/licenses/by/4.0/).

1. Introduction

Titanium and its alloys, along with aluminum and its alloys, are materials that are experiencing a growing application in modern industry [1,2]. Their use in the automotive industry and in the aircraft construction industry is of particular significance to the research community [3–6]. Aluminum and titanium are characterized by their lightweight structure—the density of titanium is 4507 kg/m^3 and that of aluminum is 2700 kg/m^3 [7], which leads to a reduction of fuel consumption and pollution in the environment. At the same time, they are characterized by superior mechanical properties, and therefore, the welding and joining of these materials are of major importance for modern industry since lightweight structures with excellent mechanical properties can be obtained.

The joining of Ti- and Al-based alloys is considered difficult due to the different thermophysical and thermochemical properties of both kinds of materials [8,9]. Welding of Ti and Al alloys leads to the formation of intermetallic structures, such as Ti_3Al, TiAl, and $TiAl_3$, in the welded seam that are characterized as very brittle, leading to fracturing the welded joint. This problem makes the joining of titanium- and aluminum-based materials challenging.

A number of methods for welding and joining exist, namely, friction stir welding [10–15], diffusion welding [16–19], explosive welding [20–22], laser beam welding [23–26], and electron beam welding [27–32]. In Ref. [13], the joining of Ti and Al was realized by friction stir welding. The results demonstrated the existence of the $TiAl_3$ phase, and the mechanical strength reached 68% of the strength of aluminum. In Ref. [19] was demonstrated the possibility of joining Ti6Al4V and aluminum by diffusion welding. It was found that the hardness decreases from the joint to the Ti part of the specimen, while at Al it remains constant. The authors of [20] investigated the joining of Al/Ti by explosive welding technology. Their results showed the existence of $TiAl_3$, TiAl, and Ti_3Al phases in which the microstructure is significantly finer in comparison with the base materials. The authors of [23] demonstrated the joining of dissimilar aluminum alloy AA6056 and titanium alloy Ti6Al4V by laser beam welding, and the results showed a significantly refined microstructure of the joint with higher hardness and strength. Electron beam welding technology demonstrates many advantages in comparison with the other welding methods, such as the higher efficiency of the electron beam, a very short process time, low cost, and others [30–33]. In addition, the process of electron beam welding (EBW) is carried out in a vacuum environment that hinders the formation and implementation of the impurities of oxide compounds in the structure of the weld seam. This effect guarantees the quality and reproducibility of the structure of the joint. The high applicability of this method is confirmed by previous research, which indicates that due to the very high energy density and efficiency of the process, the formation of narrower heat-affected zones is possible compared to other methods [30–33].

A popular method used in order to improve the process of welding dissimilar metals, particularly with such greatly different thermophysical properties, is the offset (shifting) of the beam from the basic trajectory between the two weld pieces towards one that follows one of the substrates more closely [34–36]. Using this technological condition, it is theoretically possible to controllably obtain weld joints with different microstructures. The authors of [37] investigated the interfacial morphology of the Ti-2024Al alloy joint welded by electron beam welding, in which the beam offset was towards the Al alloy. Also, the welds were realized with and without Al-5Mg alloy filler wire. The results showed that a $TiAl_3$ interfacial layer was obtained in both considered cases. Also, the application of the filler wire has led to a homogeneous distribution of the thermal field, leading to the diffusion of Ti atoms at the bottom of the seam, which is the main reason for the enhancement of the strength of the joint. Similarly, in Ref. [38], the weldability of Ti6Al4V and 6061-Al alloys was investigated. The results showed that the application of an offset strongly influences the phase composition and hardness of the obtained joint, where the maximum offset was 0.3 mm. However, this offset is very close to the diameter of the electron beam. This fact, together with the application of oscillation during the welding procedure, leads to the interaction of the electron beam with both welded plates.

The performed literature review shows that the electron beam welding technology is very promising for welding metals and alloys with different thermophysical properties. Moreover, the offsetting of the electron beam is of major importance for controlling the structure and functional properties of the welded joints. However, a detailed investigation on the structural formation of welded joints between Ti6Al4V and 6082-T6 Al-based alloys formed by a scanning electron beam, as well as the influence of the beam offset on the structure and properties of the weld seam, are currently less well investigated. Moreover, no data on EBW with higher than 0.3 mm offset are presented within the scientific literature. As mentioned previously, the implementation of an electron beam with an offset of 0.3 mm

results in the interaction of the beam with both substrates, since the diameter of the beam itself is close to that of the set offset. However, by further increasing the offset, interaction with one of the substrates is minimized, leading to very different processes occurring within the weld pool.

Therefore, the goal of this research is to provide insight into the influence of the electron beam offset of 0.5 mm on the resultant microstructure and mechanical properties of dissimilar welds between the Ti6Al4V (Ti64) and Al6082-T6 alloys.

2. Materials and Methods

As mentioned above, this study is based on the formation of dissimilar welds between commercial Ti64 and Al6082-T6 alloys. Their chemical composition is shown in Table 1.

Table 1. Chemical composition of the welded alloys.

Element, wt.%	**Al**	**V**	**Fe**	**Ti**	**-**
Ti6Al4V	5.5–6.5	3.5–4.5	0.25	Bal.	-
Element, wt.%	**Si**	**Mn**	**Mg**	**Fe**	**Al**
Al6082-T6	0.7–1.3	0.4–1.0	0.6–1.2	0.5	Bal.

In order to obtain the necessary weld joints, three butt joints were performed on welding plates with a length of 100 mm, a width of 50 mm, and a thickness of 8 mm. The first weld joint (Sample 1) was formed using a standard non-deflected electron beam. Sample 2 was obtained by offsetting the electron beam towards the titanium substrate with a beam offset d (mm) of 0.5 mm. According to the previous methodology, Sample 3 was obtained by deflecting the electron beam 0.5 mm toward the aluminum substrate. A scheme of the experiment is shown in Figure 1.

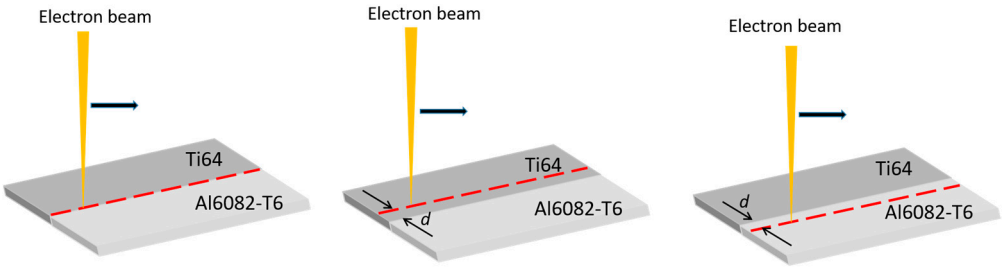


Figure 1. Schematic of the process of EBW of Ti64 and Al6082-T6.

All experiments were carried out on an electron beam installation Evobeam Cube 400, manufactured by Evobeam GmbH, Nieder-Olm, Germany. The employed technological conditions during the electron beam welding process are summarized in Table 2. A constant beam power of 2100 W was used in all cases. The welding speed was also constant with a value of 10 mm/s. The process parameters used in this work were optimized after a number of experiments. It was found that a lower beam current or a higher speed of the motion of the workpieces does not lead to a weld with full penetration. At the same time, a higher beam current or lower speed of the specimen's motion leads to the flow of the weld. The selected process parameters and technological conditions were considered the most representative.

X-ray diffraction experiments (XRD) were employed to investigate the phase composition of the welded specimens. The experiments were realized in a symmetrical Bragg–Brentano mode from 30 to 90 degrees at a 2θ scale with a step of 0.05° and a counting time of 1s per step. The measurements were carried out using CuKα radiation with a wavelength of λ = 1.54060 Å on a diffractometer "Bruker D8 Advance," Brucker Corp., Billerica, MA, USA.

Table 2. Technological parameters of the process of EBW of Ti64 and Al6082-T6.

Sample	Accelerating Voltage U, kV	Beam Current I, mA	Welding Speed v, mm/s	Offset d, mm
# 1	60	35	10	0
# 2	60	35	10	+0.5
# 3	60	35	10	−0.5

In order to study the microstructure of the weld seams, metallographic samples of the cross-section of the weld seams were prepared. The samples were mechanically polished and etched using a combination of HF and HNO_3 acid. Subsequently, scanning electron microscopy (SEM) was used to study the microstructure of the investigated samples. The SEM images were obtained via a microscope "LYRA I XMU," Tescan Orsay Holding, a.s., Kohoutovice, Czech Republic, using secondary and backscattered electrons.

Energy-dispersive X-ray spectroscopy (EDX) utilizing a "Quantax 200," Brucker Corp., Billerica, MA, USA, was used for the determination of the elemental distribution of the samples.

The Vickers hardness of the samples is indicative of the obtained microstructures during the welding process. The microhardness was measured on a semi-automatic microhardness tester, "ZWICK/Indentec-ZHVμ-S," ZwickRoell GmbH & Co. KG, Ulm, Germany, in the middle of the weld seam following a linear path perpendicular to the cross-section of the weld seam. A constant loading force of 0.5 N was applied in all cases during the experiment. The measurements were realized according to the ISO 6507-1 standard. The distance between each indentation was more than three times the diagonals of the indentations, and the criteria were fulfilled. The dwell time in all microhardness determination experiments was 10 s.

The tensile strength and yield stress were determined from tensile tests at room temperature by means of a Zwick/Roell Vibrophore 100, ZwickRoell GmbH & Co. KG, Ulm, Germany, testing machine with constant rate of stresses in the elastic region of 30 MPa/s in accordance with the ISO 4136 standard.

3. Results

Cross-sectional SEM images of the welded samples are shown in Figures 2–4. Figure 2a presents the formed weld seam using a non-deflected electron beam. The obtained weld seam consists of a mixture of both the Ti64 and the Al6082-T6 alloys. A noticeable pore within the fusion zone is observed, along with some solidification pores, formed during the welding process, which can be seen in Figure 2b,d, primarily on the aluminum side. Figure 2c shows the clearly visible border of the heat-affected zone. This appearance is confirmed by the EDX analysis, which indicates that the chemical composition of the fusion zone consists of 75.7 wt.% Ti, 23.1 wt.% Al, and 1.2 wt.% V, corresponding to Point 1 of Table 3. In comparison, the studied zone on the right (corresponding to Point 2) consists of 91.9 wt.% Ti, which indicates that whether during the welding process or during the process of sample preparation some aluminum atoms have been diffused to the Ti64 substrate; however, the high concentration of Ti64 is enough to conclude that the material observed in that zone is indeed Ti64 in which some amount of aluminum exists. The elemental ratio of Ti–Al measured within Points 4 and 5 from Figure 2e and summarized in Table 3 is equal to 70.0–28.4 and 63.5–35.0 (in wt.%), which, according to the binary phase diagram in the system of Ti–Al, corresponds to the γ-TiAl phase [39,40].

Similar to Sample 1, Figure 3a shows the seam formed during welding of the substrates with an offset of the electron beam towards the Ti6Al4V welding plate. Two large pores can be observed in the structure of this specimen as well, accompanied by some solidification pores observed in Figure 3b,e,f. Figure 3b shows a border between the Al plate and the seam, and it is obvious that the region consists mostly of Al (Points 14 and 12 from Table 4), and some intermetallic fractions can be seen (Point 13 from Table 4). According to the

binary phase diagram, Point 13 corresponds to the γ-TiAl phase [39,40]. Figure 3c shows the border of the heat-affected zone towards the Ti64 side. Evidently, it is not as well defined as compared to the one observed in the previous sample. The application of the offset towards the Ti64 alloy leads to the formation of two distinguished zones within the welded joint. In this case, a lesser amount of material is melted, since the melting point of Ti6Al4V is much higher than that of the aluminum alloy. Moreover, the lifetime of the molten material is shorter, leading to worse miscibility within the fusion zone. Similar features were observed also in the EBW of Cu to stainless steel [29]. Figure 3d–g shows zoomed-in images of the fusion zone along with the zones where the energy-dispersive X-ray spectroscopy was performed. The results of that experiment are summarized in Table 4. The most commonly detected distribution of elements within the intermetallic phases corresponds to the γ-TiAl phase. However, some intermetallic formations with a ratio between Ti–Al exist belonging to the α_2-Ti_3Al and Al_3Ti phases (Points 7 and 11 for α_2-Ti_3Al and Point 13 for Al_3Ti) [39,40]. It is important to note that both considered welded joints exhibit large pores at the center of the seam. As it is known, the process of electron beam welding incorporates highly uneven fluid dynamics processes due to highly inhomogeneous thermal fields throughout the welding seam [41,42]. Previous research also indicates that the highest observed thermal gradients during electron beam welding are at the top of the weld seam during the process, due to the higher dissipation of kinetic energy in the first stages of the penetration of the electrons [43]. The higher thermal gradient indicates that the speed of solidification at the top of the weld pool is substantially higher compared to the ones at the root of the seam. In addition, Ti64 and Al6082-T6 have completely different thermophysical properties, which results in a different flow of the molten materials during the welding stage. Since titanium and its alloys have a much lower thermal conductivity compared to aluminum, the process of solidification becomes faster towards the aluminum substrate. The rapid solidification of the aluminum incorporation in the weld seam leads to the formation of large pores in the space between the aluminum and the titanium specimens (between points 8 and 9, as well as around point 10). The existence of such macro defects could be considered a drawback of the functional properties of the welded joint since it is expected to deteriorate the mechanical properties.

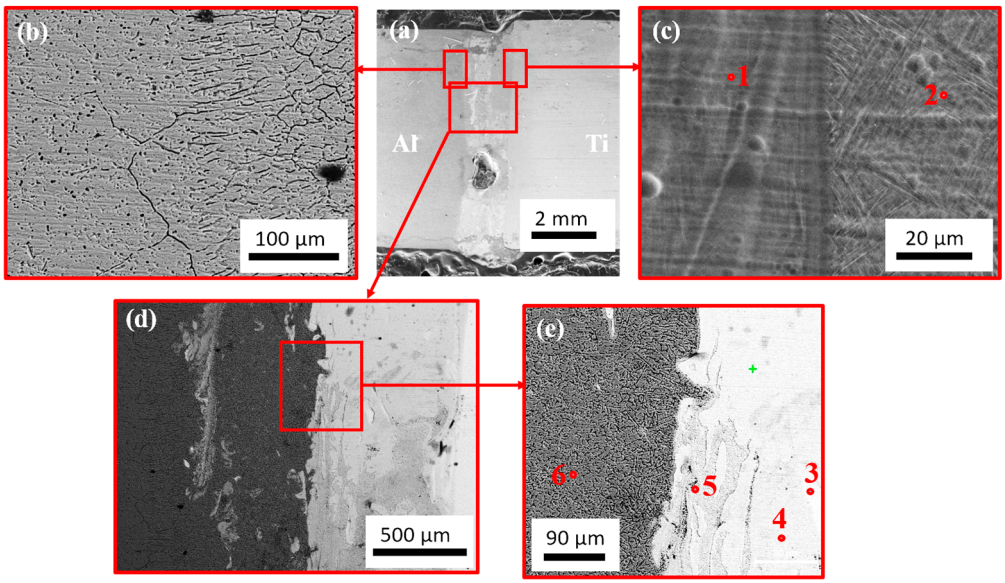


Figure 2. Cross-sectional SEM images of the sample welded without a beam offset (Sample1): (**a**) SEM image of the obtained joint; (**b**) higher magnification SEM image of the interface aluminum alloy—fusion zone; (**c**) interface fusion zone—titanium alloy; (**d**,**e**) fusion zone.

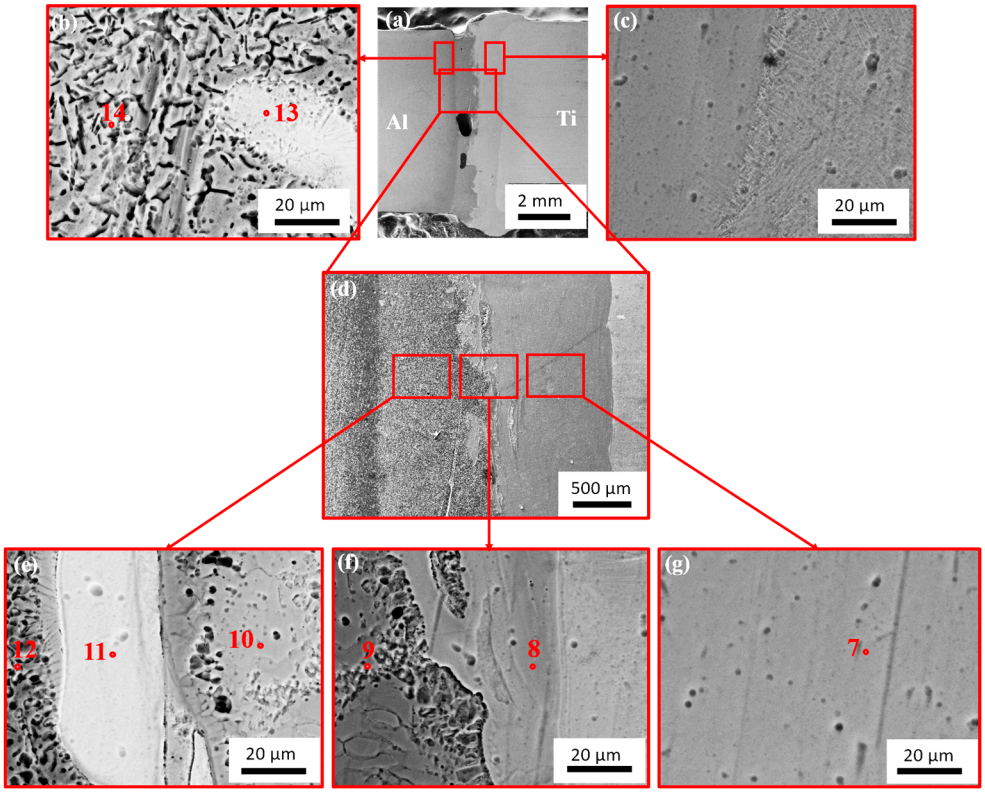


Figure 3. Cross-sectional SEM images of the sample welded with a beam offset toward Ti64 (Sample 2): (**a**) SEM image of the obtained joint; (**b**) higher magnification SEM image of the interface aluminum alloy—fusion zone; (**c**) interface fusion zone—titanium alloy; (**d**) fusion zone; (**e**) fusion subzone close to the aluminum alloy plate; (**f**) middle of the fusion zone; (**g**) fusion subzone close to the titanium alloy plate.

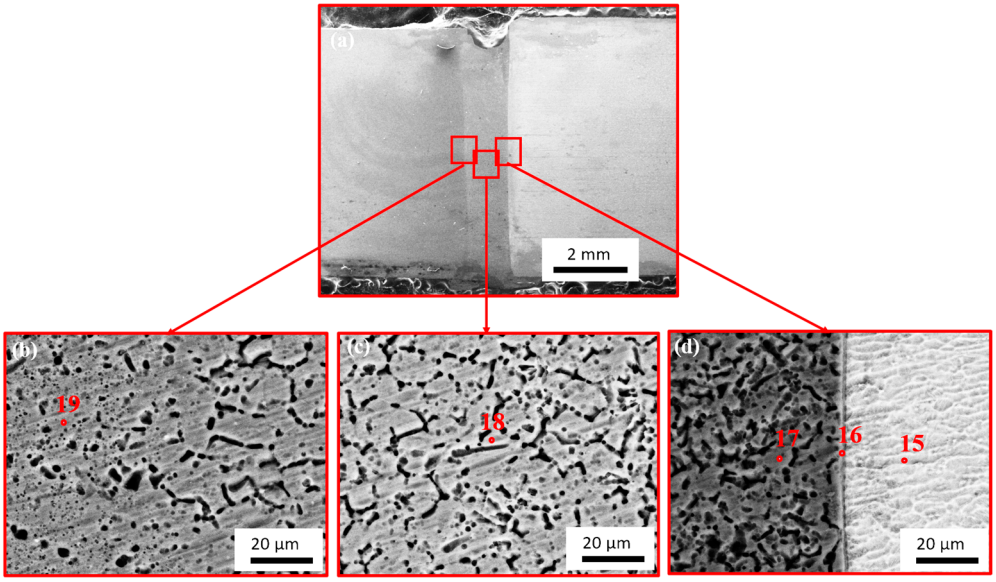


Figure 4. Cross-sectional SEM images of the sample welded with a beam offset toward Al6082-T6 (Sample 3): (**a**) SEM image of the obtained joint; (**b**) higher magnification SEM image of the interface aluminum alloy—fusion zone; (**c**) fusion zone; (**d**) interface fusion zone—titanium alloy.

Table 3. Chemical composition and assumptions of the potentially detected phases within the fusion zone of Sample 1.

	Point 1	Point 2	Point 3	Point 4	Point 5	Point 6
Ti, wt.%	75.7 ± 2.2	91.9 ± 3.3	86.7 ± 2.9	70.0 ± 2.2	63.5 ± 2.2	0.3 ± 0.1
Al, wt.%	23.1 ± 1.0	5.9 ± 0.3	11.2 ± 0.6	28.4 ± 1.3	34.9 ± 1.7	99.68 ± 4.4
V, wt.%	1.2 ± 0.7	2.3 ± 1.5	2.0 ± 1.4	1.6 ± 1.0	1.5 ± 1.0	0.6 ± 0.1

Table 4. Chemical composition of each point marked on the SEM images of Sample 2 in Figure 3.

	Point 7	Point 8	Point 9	Point 10	Point 11	Point 12	Point 13	Point 14
Ti, wt.%	88.6 ± 3.9	68.6 ± 4.8	55.4 ± 3.8	58.6 ± 4.4	83.5 ± 5.1	6.2 ± 0.6	46.7 ± 3.7	3.3 ± 0.3
Al, wt.%	14.9 ± 0.8	28.2 ± 1.4	42.6 ± 2.0	39.2 ± 1.9	13.8 ± 0.8	92.9 ± 4.0	51.7 ± 2.5	95.3 ± 4.8
V, wt.%	2.5 ± 1.6	3.2 ± 2.0	2.4 ± 1.3	2.3 ± 1.5	2.7 ± 1.8	0.9 ± 0.6	1.8 ± 1.2	1.3 ± 0.8

Figure 4a shows the electron beam weld produced by offsetting the electron beam toward the aluminum plate and Table 5 presents the Chemical composition of each point marked on SEM images. This offset resulted in highly accelerated melting processes of that substrate and a very poor melting of the Ti64 one. This result means that most of the fusion zone (Figure 4c, Point 18) and the heat-affected zone formed closer toward the aluminum (Figure 4b, Point 19) specimen consists of aluminum and a very small percentage of Ti64, which was incorporated in it via the observed diffusion processes. Only a small fusion zone at the border between the melted zone and the Ti64 substrate was observed. The results obtained by the EDX investigations show that the elemental composition of this zone is 17.4 wt.% Ti, 81.9 wt.% Al, and 0.7 wt.% V (Point 16), which according to the Ti–Al phase diagram corresponds to the $TiAl_3$ phase [39,40]. Due to the high thermal conductivity of aluminum, and due to its high coefficient of thermal expansion during the cooling stage of the melt pool, a high concentration of solidification pores was observed. According to the authors of [44], the thermal gradient during the manufacturing processes is directly correlated with the solidification speed, which in turn is related to the formation speed of solidification pores. With the increase in the thermal gradient, the formation of the solidification pores increases as well, as shown in Ref. [44]. The higher coefficient of thermal expansion of the Al alloy, as compared to other metals and alloys such as Ti, steels, etc., favors the formation of the discussed porosity (Point 17). However, no macro-pores, such as in the cases of beam offsetting towards the Ti alloy and the weld without shifting the beam, can be observed, which could be considered as an advantage for the resultant functional properties (Point 15).

Table 5. Chemical composition of each point marked on SEM images of Sample 3 in Figure 4.

	Point 15	Point 16	Point 17	Point 18	Point 19
Ti, wt.%	90.3 ± 5.3	17.4 ± 1.6	0.6 ± 0.1	0.8 ± 0.1	0.3 ± 0.1
Al, wt.%	6.7 ± 0.4	81.9 ± 3.6	99.0 ± 4.4	98.7 ± 4.2	99.3 ± 4.1
V, wt.%	3.0 ± 1.9	0.7 ± 0.4	0.4 ± 0.3	0.5 ± 0.3	0.4 ± 0.2

In Figure 5, the X-ray diffraction patterns for the studied samples are presented. All diffraction maxima are indexed. It is well visible that for all considered specimens, besides peaks corresponding to pure Ti and Al, diffraction maxima of intermetallic phases in the system of Ti–Al exist as well. Considering the first specimen (i.e., the welded joint without the application of an offset), the existence of γ-TiAl, as well as α_2-Ti_3Al intermetallic phases, can be observed along with the pure Ti and Al. These results are fully in agreement with those obtained by the SEM/EDX analyses, in which the studied chemical composition of different formations obtained within the welded joint point out the existence of the aforementioned phases, and with the binary phase diagram of the system of Ti–Al [39,40]. Considering the phase composition of the welded specimen by an offset of the electron

beam to the titanium plate (i.e., the second specimen), diffraction maxima of pure Ti and Al are observed. Additionally, peaks of many intermetallics are visible, namely γ-TiAl, α_2-Ti_3Al, and $TiAl_3$. In this case, both metals are intensively melted, and the melt pool consists of both materials, resulting in the formation of a high quantity of intermetallics. The phase composition of the third specimen (i.e., a welded joint with an offset towards the Al alloy) is in the form of pure Al, and small peaks of the $TiAl_3$ are observable, meaning that a small amount of this phase exists. In this case, only the Al alloy is melted, and some amount of Ti atoms diffuse to the molten aluminum, leading to the formation of a very narrow intermetallic area, as shown in Figure 4d. Peaks corresponding to pure Ti are also visible at the discussed diffraction pattern. As already mentioned, the obtained fusion zone is too narrow, even narrower than the dimension of the X-ray spot, and during the measurement, some area of the Ti alloy also appears.

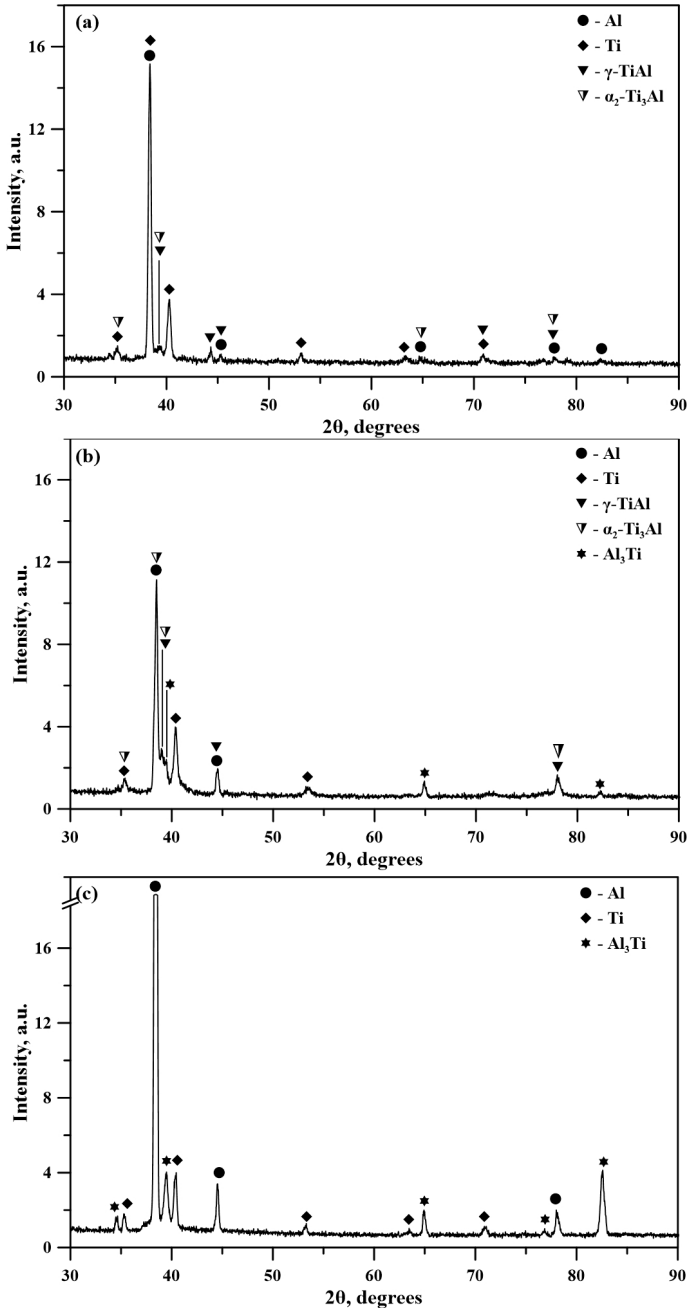


Figure 5. X-ray diffraction patterns of the welded joints: (**a**) without offset; (**b**) with an offset towards the Ti alloy; (**c**) with an offset towards the Al alloy.

As previously mentioned, the microhardness of the samples was measured perpendicular to the fusion/melt zone. The results of the experiment are shown in Figure 6. Figure 6a–c corresponds to the samples formed using an electron beam without offset, with offsetting towards the Ti64 substrate and the aluminum substrate. In the first two cases, an average microhardness of the aluminum substrate of about 75 $HV_{0.05}$ was obtained. The microhardness of the aluminum substrate in the case of welding with an electron beam offset towards the aluminum substrate is 95 $HV_{0.05}$. In regards to the Ti64 substrate, a microhardness of about 380 $HV_{0.05}$ was observed in all cases. These results are comparable with those obtained by the authors of [45], in which the hardness of the Ti6Al4V alloy has been studied. The microhardness curve of Sample 1 is characterized by some spikes in the microhardness, which, however, do not exceed (or only exceed slightly) the microhardness of the Ti6Al4V alloy. These spikes can be attributed to an increase in the concentration of intermetallics in the area of measurement. The same tendency is observed considering Sample 2, which was formed by offsetting the beam towards the Ti64 specimen. The values of the microhardness measured in the fusion zone exceed greatly the ones measured for both the Al alloy and the Ti64 substrates. This result is once again attributed to the increased concentration of intermetallics in that zone. It should be noted that in this case the existence of the $TiAl_3$ phase is observed, which is characterized by a very high hardness, and therefore, this rise in the discussed mechanical characteristic could be attributed to the existence of the above-mentioned compound. Sample 3 is characterized by a sudden change in the Vickers hardness. Due to the poor integration of Ti into the structure of the fusion zone, the microhardness in that area is the same as that of the Al substrate. A rapid increase is noticed when the indenter tip reaches the Ti64 substrate.

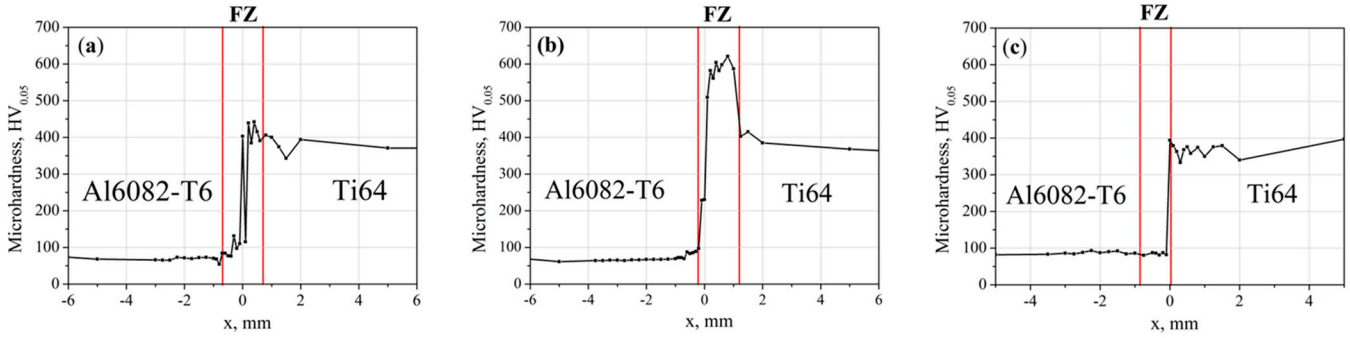


Figure 6. Microhardness distribution across the weld formed using: (**a**) no beam offset, (**b**) beam offset toward Ti64, (**c**) beam offset toward Al6082-T6. (FZ—fusion zone).

The results obtained for tensile strength (TS) and yield strength (YS) are presented in Figure 7. It is well visible that the welding without the application of an offset is characterized by lower values of the discussed mechanical characteristic, for which the measured values are about 74 MPa for both mechanical characteristics (i.e., TS and YS). The application of an offset leads to an increase in the measured values, which, in the case of the shifting of the beam towards the Ti64 alloy, the TS is 128 MPa and the YS is 124 MPa. The application of an offset towards the Al6082-T6 alloy leads to the highest measured values of 157 MPa and 152 MPa for the TS and YS, respectively. The influence of the phase composition and microstructure on the measured mechanical properties is significant. As already mentioned, the amount of intermetallic phases is the lowest in the case of offsetting towards the Al alloy, which is the main reason for the significant enhancement of the tensile strength and yield strength. The other two welded joints are characterized by a significantly larger amount of intermetallic phases that are characterized as very brittle, leading to deterioration in the mechanical characteristics. Moreover, both seams, without offsetting and with offsetting towards the Ti64 alloy, presented macro-pores which also have a negative effect on the considered mechanical properties.

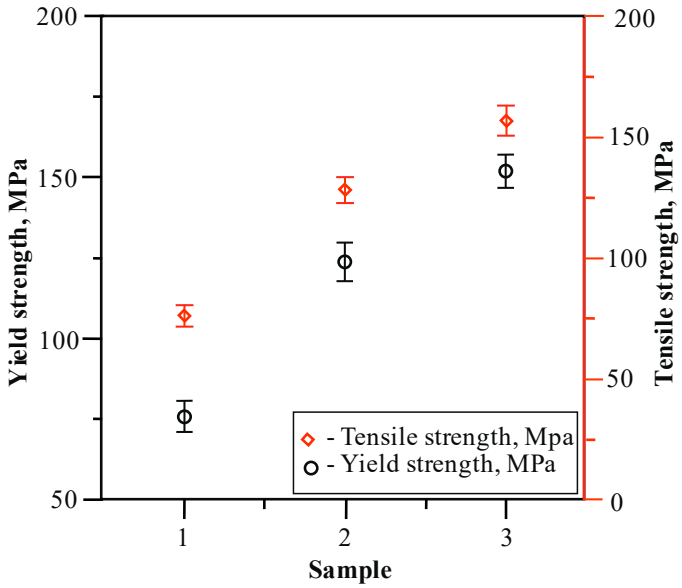


Figure 7. Mechanical properties of the welded joints characterized by tensile experiments: Sample 1—without offset; 2—0.5 mm offset towards the Ti6Al4V alloy; 3—0.5 mm offset towards the Al6082-T6 alloy.

4. Discussion

The subject of the present work is the investigation of the effect of electron beam offset on the structure and microhardness of electron-beam-welded titanium- and aluminum-alloy specimens. Due to the high input power of the electron beam, full penetration of the substrates was achieved in all cases, as opposed to the formation of a standard "keyhole" type of weld. This result is, however, beneficial due to the formation of narrow and symmetrical heat-affected zones.

The results obtained in the present study show that the offset of the electron beam has a significant influence on the structure and properties of the obtained welded joints. During the welding process without offsetting or with an application of an offset towards the Ti6Al4V alloy, the formed seams are characterized by a significant inhomogeneity in which a large amount of intermetallic fractions are observed. However, the application of the offset of the electron beam towards the Al6082-T6 alloy leads to the formation of a welded joint consisting mostly of pure Al, and a very narrow layer in the form of an intermetallic structure is observable, which can be considered as a serious advantage over the other two cases. During the electron beam welding of the Ti6Al4V and Al6082-T6 alloys, when the welding procedure was realized without offset or with a shift of the beam towards the Ti-based alloy, both alloys are extensively melted due to the significantly lower thermal conductivity of the Ti64. In this case, the molten pool consists of both types of welded materials, leading to the formation of a significant amount of intermetallic structures. The weld pool is characterized by a very high thermal gradient, leading to the formation of convection flows acting from the surface to the bulk of the weld pool [46]. These convection flows are responsible for the introduction and mixing of the materials within the molten pool and lead to the formation of intermetallic structures [47–49]. These statements are in agreement with the results obtained in the present study, in which a significant amount of intermetallic phases in the system of Ti–Al were formed under the present technological conditions (determined by the offset). In the case of shifting the beam towards the aluminum alloy, the weld pool consists mostly of Al since the thermal conductivity of the Al alloy is significantly higher than that of the Ti6Al4V alloy, and the temperature at the interface between both materials is insufficient to melt the titanium alloy or only melts a very small area of it. The thermal gradient and corresponding convection flows are not responsible for the introduction of a significant amount of Ti material into

the weld pool and the mixing of both alloys. Therefore, the intermetallic structures within the welded joint are greatly reduced, as in the present particular case; they are in the form of a very thin layer at the interface between the Ti and Al alloys. As mentioned in the introduction, the authors of [38] studied the weldability of the Ti6Al4V and 6061-Al alloys. The results showed that the application of an offset strongly influences the phase composition and hardness of the obtained joint, where the maximum offset was 0.3 mm. However, this offset is very close to the diameter of the electron beam, and this leads to the interaction of the electron beam with both welded plates. As a result, the structure investigated in Ref. [38] for a welded joint in which the beam has been shifted towards the Al alloy is much wider and consists of a large number of intermetallic phases, which is expected to lead to a deterioration in the functional properties. Therefore, the application of a larger offset (two times larger than the beam spot in the present case) to the material with the lower melting point and higher thermal conductivity has a major importance and plays a very important role in the reduction of the intermetallic structures. Similarly, the limited mixture of both materials leads to the suppression of the formation of macro-pores. It is well known that Ti64 and Al6082-T6 have completely different thermophysical properties, and since titanium and its alloys have a much lower thermal conductivity compared to aluminum, the process of solidification becomes faster towards the aluminum substrate. The rapid solidification of the aluminum incorporation in the weld seam leads to the formation of large pores in the space between the aluminum and the titanium specimens. The existence of such macro defects could be also considered as a drawback of the functional properties of the welded joint since it is expected to deteriorate the mechanical properties.

These statements were confirmed by the investigation of the mechanical properties. It was demonstrated that the microhardness of the obtained welded joints is much higher than that of the Al alloy and is comparable with that of the Ti alloy. The welded joint with an offset to the Ti-based material exhibits the highest value of microhardness due to the significant amount of brittle and hard intermetallic titanium aluminides. However, as already mentioned, this amount makes the welded joint brittle, which still limits the number of applications. At the same time, the microhardness of the specimen welded by an offset towards the Al material is lower in comparison with that welded by the shift of the beam towards the Ti alloy but has better tensile properties.

5. Conclusions

In this study, the possibility of electron beam welding of Al6082-T6 and Ti6Al4V alloys was investigated. The experiments were realized by an offset of the electron beam towards both alloys, as well as without the application of an offset. The offset of the electron beam has a significant effect on the structure of the weld. The following conclusions can be drawn:

- In non-offset welding and when the beam is shifted to titanium, a liquid–liquid reaction occurs, while when the beam is shifted to aluminum, a liquid–solid reaction occurs.
- The welding procedure without offset and with an offset towards the Ti alloy leads to inhomogeneous welded joints with a significant amount of intermetallics. The formed fusion zones of these specimens are much larger than that of the weld with an offset towards the Al alloy.
- In the case of welding without an offset, two intermetallic phases are formed—γ-TiAl and α_2-Ti_3Al. The welded seam of the second specimen (i.e., with an offset towards the Ti alloy) consists of the largest number of intermetallics, namely γ-TiAl, α_2-Ti_3Al, and $TiAl_3$. The third one (i.e., with an offset towards the Al alloy) consists of only a narrow area of the $TiAl_3$ phase.
- The measured microhardness corresponds to the increased amount of intermetallics in the case of offset towards the Ti alloy, with which the highest values were presented (more than 600 HV or 58% higher than the Ti6Al4V plate). The hardness of the welds formed without an offset, as well as with an offset towards the Al alloy, is lower and is close to that of the Ti6Al4V material.

- The results obtained for tensile properties show that the offset to the Al6082-T6 alloy leads to the highest values of tensile strength (TS) and yield strength (YS). The measured values for TS and YS are 157 MPa and 152 MPa, respectively, which is twice higher than for the weld without offsetting of the electron beam.

Author Contributions: Conceptualization, D.K., A.A. and S.V.; methodology, D.K.; validation, A.A., M.O. and S.V.; formal analysis, G.K., V.D. and D.K.; investigation, V.D., B.S., M.A., V.T. and P.D.; resources, B.S., M.A. and V.T.; data curation, G.K., P.D. and M.O.; writing—original draft preparation, G.K. and D.K.; writing—review and editing, G.K. and S.V.; visualization, M.O. and M.A.; supervision, D.K.; project administration, A.A. and D.K.; funding acquisition, A.A. and D.K. All authors have read and agreed to the published version of the manuscript.

Funding: This work was supported by the Bulgarian National Scientific Fund under Grant KP 06-N-47/6.

Data Availability Statement: Not applicable.

Conflicts of Interest: The authors declare no conflict of interest.

References

1. Saurabh, A.; Meghana, M.; Singh, K.; Verma, C. Titanium-based materials: Synthesis, properties, and applications. *Mat. Today Proc.* **2022**, *56*, 412–419. [CrossRef]
2. Stojanovic, B.; Bukvic, M.; Epler, I. Application of aluminum and aluminum alloys in engineering. *Appl. Eng. Let. J. Eng. Appl. Sci.* **2018**, *3*, 52–62. [CrossRef]
3. Schauerte, O. Titanium in automotive production. *Adv. Eng. Mat.* **2003**, *5*, 411–418. [CrossRef]
4. Williams, J.; Boyer, R. Opportunities and issues in the application of titanium alloys for aerospace components. *Metals* **2020**, *10*, 705. [CrossRef]
5. Kumar, V.; Gupta, R.; Prasad, M.; Murty, S. Recent advances in processing of titanium alloys and titanium aluminides for space applications: A review. *J. Mater. Res.* **2021**, *36*, 689–716. [CrossRef]
6. Makai, M.; Eto, T. New aspect of development of high strength aluminum alloys for aerospace applications. *Mat. Sci. Eng. A* **2000**, *285*, 62–68.
7. Cverna, F. *ASM Ready Reference: Thermal Properties of Metals*; ASM International: Materials Park, OH, USA, 2002.
8. Kim, Y.-C.; Fuji, A. Factors Dominating Joint Characteristics in Ti-Al Friction Welds. *Sci. Technol. Weld. Join.* **2002**, *7*, 149–154. [CrossRef]
9. Chen, S.; Li, L.; Chen, Y.; Dai, J.; Huang, J. Improving interfacial reaction nonhomogeneity during laser welding–brazing aluminum to titanium. *Mater. Des.* **2011**, *32*, 4408–4416. [CrossRef]
10. Abdollahzadeh, A.; Bagheri, B.; Shamsipur, A. Development of Al/Cu/SiC bimetallic nano-composite by friction stir spot welding. *Mater. Manuf. Proc.* **2022**, *38*, 1416–1425. [CrossRef]
11. Abdollahzadeh, A.; Bagheri, B.; Abbasi, M.; Sharifi, F.; Mirsalehi, S.E.; Moghaddam, A.O. A modified version of friction stir welding process of aluminum alloys: Analyzing the thermal treatment and wear behavior. *Proc. Inst. Mech. Eng. Part L J. Mater. Des. Appl.* **2021**, *235*, 2291–2309. [CrossRef]
12. Abbasi, M.; Bagheri, B.; Abdollahzadeh, A.; Moghaddam, A. A different attempt to improve the formability of aluminum tailor welded blanks (TWB) produced by the FSW. *Int. J. Mater. Form.* **2021**, *14*, 1189–1208. [CrossRef]
13. Wi, A.; Song, Z.; Nakata, K.; Liao, J.; Zhou, L. Interface and properties of the friction stir welded joints of titanium alloy Ti6Al4V with aluminum alloy 6061. *Mater. Des.* **2015**, *71*, 85–92.
14. Ataya, S.; Ahmed, M.M.Z.; El-Sayed Seleman, M.M.; Hajlaoui, K.; Latief, F.H.; Soliman, A.M.; Elshaghoul, Y.G.Y.; Habba, M.I.A. Effective Range of FSSW Parameters for High Load-Carrying Capacity of Dissimilar Steel A283M-C/Brass CuZn40 Joints. *Materials* **2022**, *15*, 1394. [CrossRef] [PubMed]
15. Ahmed, M.M.Z.; Ataya, S.; El-Sayed Seleman, M.M.; Mahdy, A.M.A.; Alsaleh, N.A.; Ahmed, E. Heat Input and Mechanical Properties Investigation of Friction Stir Welded AA5083/AA5754 and AA5083/AA7020. *Metals* **2021**, *11*, 68. [CrossRef]
16. John, B.; Letsch, H.; Wölck, J.; Hess, M.; Hensel, J. Process Technology for Diffusion Welding with Cyclically Pulsative Joining Forces. *Metals* **2023**, *13*, 547. [CrossRef]
17. Zhang, Y.; Zhao, T.; Yu, X.; Huang, J. The Al-Fe Intermetallic Compounds and the Atomic Diffusion Behavior at the Interface of Aluminum-Steel Welded Joint. *Metals* **2023**, *13*, 334. [CrossRef]
18. Chiang, M.-T.; Chiu, K.-Y.; Wu, P.-C.; Chang, S.-Y.; Sun, Y.-K.; Chuang, T.-H. Improvement of the Mechanical Properties of the Diffusion-Bonded 2024 Aluminum Alloy through Post-Weld Heat Treatments. *Metals* **2022**, *12*, 1738. [CrossRef]
19. Akca, E.; Gursel, A. The Effect of Diffusion Welding Parameters on the Mechanical Properties of Titanium Alloy and Aluminum Couples. *Metals* **2017**, *7*, 22. [CrossRef]

20. Fronczek, D.M.; Chulist, R.; Litynska-Dobrzynska, L.; Szulc, Z.; Zieba, P.; Wojewoda-Budka, J. Microstructure Changes and Phase Growth Occurring at the Interface of the Al/Ti Explosively Welded and Annealed Joints. *J. Mater. Eng. Perform.* **2016**, *25*, 3211–3217. [CrossRef]
21. Zhou, Q.; Lu, H.; Zhang, Y.; Guo, Y.; Zhu, L.; Huang, G.; Chen, P. Intermetallic Reaction of the Bonding Interface of TA2/Q235 Explosive Welding Composite. *Metals* **2023**, *13*, 571. [CrossRef]
22. Malyutina, Y.N.; Anisimov, A.G.; Popelyukh, A.I.; Lozhkin, V.S.; Bataev, A.A.; Bataev, I.A.; Lukyanov, Y.L.; Pai, V.V. Microstructure and Properties of Multilayer Niobium-Aluminum Composites Fabricated by Explosive Welding. *Metals* **2022**, *12*, 1950. [CrossRef]
23. Vaidya, W.V.; Horstmann, M.; Ventzke, V.; Petrovski, B.; Koçak, M.; Kocik, R.; Tempus, G. Improving interfacial properties of a laser beam welded dissimilar joint of aluminium AA6056 and titanium Ti6Al4V for aeronautical applications. *J. Mater. Sci.* **2010**, *45*, 6242–6254. [CrossRef]
24. Liu, J.; Guo, S.; Zhang, P.; Ma, T.; Wang, Z.; Wu, T.; Wang, L.; Wang, K. A Novel Approach of Microstructure Refinement of TiAl in Laser Beam Welding. *Metals* **2023**, *13*, 7. [CrossRef]
25. Song, D.; Kim, R.; Choi, K.; Shin, D.; Lee, S. Effects of Beam Shape on the Microstructures and Mechanical Properties during Thin-Foil Laser Welding. *Metals* **2023**, *13*, 916. [CrossRef]
26. Xu, B.; Jin, G.; Zhang, Z.; Wang, J.; Zhan, X. Effect on the Property of 2195 Al-Li Alloy Laser-Welded Joints with Different Filler Materials. *Metals* **2023**, *13*, 958. [CrossRef]
27. Kaisheva, D.; Anchev, A.; Valkov, S.; Dunchev, V.; Kotlarski, G.; Stoyanov, B.; Ormanova, M.; Atanasova, M.; Petrov, P. Influence of Beam Power on Structures and Mechanical Characteristics of Electron-Beam-Welded Joints of Copper and Stainless Steel. *Metals* **2022**, *12*, 737. [CrossRef]
28. Kotlarski, G.; Kaisheva, D.; Ormanova, M.; Stoyanov, B.; Dunchev, V.; Anchev, A.; Valkov, S. Electron-Beam Welding of Titanium and Ti6Al4V Alloy. *Metals* **2023**, *13*, 1065. [CrossRef]
29. Kaisheva, D.; Anchev, A.; Dunchev, V.; Kotlarski, G.; Stoyanov, B.; Ormanova, M.; Valkov, S. Electron-Beam Welding Cu and Al6082T6 Aluminum Alloys with Circular Beam Oscillations. *Crystals* **2022**, *12*, 1757. [CrossRef]
30. Weglowski, S.; Blacha, S.; Phillips, A. Electron beam welding—Techniques and trends—Review. *Vacuum* **2016**, *130*, 72–92. [CrossRef]
31. Kaisheva, D.; Bokuchava, G.; Papushkin, I.; Valkov, S.; Ormanova, M.; Petrov, P. Comparative neutron diffraction study of residual stresses, arising after electron beam welding of various steels. *J. Tech. Univ. Gabrovo* **2021**, *63*, 72–75.
32. Kaisheva, D.; Dunchev, V.; Kotlarski, G.; Stoyanov, B.; Ormanova, M.; Todorov, V.; Atanasova, M.; Valkov, S. Structure and Mechanical Properties of Cu/Al6082-T6 Joints Produced by Welding with Scanning Electron Beam. *J. Tech. Univ. Gabrovo* **2023**, *66*, 46–49.
33. Valkov, S.; Ormanova, M.; Petrov, P. Electron-Beam Surface Treatment of Metals and Alloys: Techniques and Trends. *Metals* **2020**, *10*, 1219. [CrossRef]
34. Guo, S.; Zhou, Q.; Kong, J.; Peng, Y.; Xiang, Y.; Lou, T.; Wang, K.; Zhu, J. Effect of beam offset on the characteristics of copper/304stainess steel electron beam welding. *Vacuum* **2016**, *128*, 205–212. [CrossRef]
35. Chen, G.; Teng, X.; Yin, Q.; Zhang, B.; Leng, X. Effect of beam offset on the microstructure and properties of a dissimilar tungsten/kovar electron beam weld. *Weld. World* **2023**, *67*, 1479–1489. [CrossRef]
36. Yeganeh, V.; Li, P. Effect of beam offset on microstructure and mechanical properties of dissimilar electron beam welded high temperature titanium alloys. *Mater. Des.* **2017**, *124*, 78–86. [CrossRef]
37. Wang, T.; Li, X.; Zhang, Y.; Li, H.; Zhang, B.; Feng, J. Regulating the interfacial morphology of electron beam welded pure Ti/2024Al dissimilar joint. *J. Mater. Proc. Technol.* **2017**, *245*, 227–231. [CrossRef]
38. Havlik, P.; Kouril, J.; Foret, R.; Dlouhy, I.; Enzinger, N.; Wiednig, C. Evaluation of Weldability of Titanium Alloy Ti-6Al-4V and Aluminum Alloy 6061 Produced by Electron Beam Welding. *Mater. Sci. Forum* **2017**, *879*, 714–719.
39. Dzogbewu, T. Additive manufacturing of TiAl-based alloys. *Manuf. Rev.* **2020**, *7*, 35. [CrossRef]
40. Okamoto, H.; Okamoto, H. *Phase Diagrams for Binary Alloys*; ASM International: Materials Park, OH, USA, 2000.
41. Luo, M.; Hu, R.; Liu, T.; Wu, B.; Pang, S. Optimization possibility of beam scanning for electron beam welding: Physics understanding and parameters selection criteria. *Int. J. Heat Mass Transf.* **2018**, *127*, 1313–1326. [CrossRef]
42. Yang, Z.; Fang, Y.; He, J. Numerical Investigation on Molten Pool Dynamics and Defect Formation in Electron Beam Welding of Aluminum Alloy. *J. Mat. Eng. Perf.* **2020**, *29*, 6570–6580. [CrossRef]
43. Petrov, P.; Tongov, M. Numerical modelling of heat source during electron beam welding. *Vacuum* **2020**, *171*, 108991. [CrossRef]
44. Sigworth, G.K.; Wang, C. Mechanisms of porosity formation during solidification: A theoretical analysis. *Met. Trans. B* **1993**, *24*, 349–364. [CrossRef]
45. Dikova, T.; Dunchev, V.; Gagov, Y. Investigation of hardness and elastic modulus of milled and SLM Ti6Al4V alloy. *J. Tech. Univ. Gabrovo* **2022**, *65*, 11–16.
46. Chan, C.; Mazumder, J.; Chen, M. A two-dimensional transient model for convection in laser melted pool. *Metall. Trans. A* **1984**, *15*, 2175–2184. [CrossRef]
47. Valkov, S.; Petrov, P.; Lazarova, R.; Bezdushnyi, R.; Dechev, D. Formation and characterization of Al–Ti–Nb alloys by electron-beam surface alloying. *Appl. Surf. Sci.* **2016**, *389*, 768–774. [CrossRef]

48. Valkov, S.; Dechev, D.; Ivanov, N.; Bezdushnyi, R.; Ormanova, M.; Petrov, P. Influence of Beam Power on Young's Modulus and Friction Coefficient of Ti–Ta Alloys Formed by Electron-Beam Surface Alloying. *Metals* **2021**, *11*, 1246. [CrossRef]
49. Ormanova, M.; Dechev, D.; Ivanov, N.; Mihai, G.; Gospodinov, M.; Valkov, S.; Enachescu, M. Synthesis and Characterization of Ti-Ta-Shape Memory Surface Alloys Formed by the Electron-Beam Additive Technique. *Coatings* **2022**, *12*, 678. [CrossRef]

Disclaimer/Publisher's Note: The statements, opinions and data contained in all publications are solely those of the individual author(s) and contributor(s) and not of MDPI and/or the editor(s). MDPI and/or the editor(s) disclaim responsibility for any injury to people or property resulting from any ideas, methods, instructions or products referred to in the content.